Crystal structure, dielectric properties, and optical bandgap control in KNbO 3 –BiMnO 3 ceramics

PASCUAL-GONZALEZ, Cristina, ELICKER, Carolina, MOREIRA, Mario L., CAVA, Sergio, STERIANOU, Iasmi, WANG, Dawei and FETEIRA, Antonio <http://orcid.org/0000-0001-8151-7009>

Received: 10 January 2022 | Revised: 4 August 2022 | Accepted: 9 August 2022

DOI: 10.1111/jace.18779

Journal of the American Ceramic Society

SPECIAL ISSUE ARTICLE

Crystal structure, dielectric properties, and optical bandgap control in $KNbO_3$–$BiMnO_3$ ceramics

Cristina Pascual-Gonzalez[1,2] | **Carolina Elicker**[1,3] | **Mario L. Moreira**[3] | **Sergio Cava**[3] | **Iasmi Sterianou**[1] | **Dawei Wang**[4] | **Antonio Feteira**[1]

[1]Materials, and Engineering Research Institute, Sheffield Hallam University, Sheffield, UK

[2]Materials Science and Engineering Area, Rey Juan Carlos University, Madrid, Spain

[3]CCAF, IFM/CDTec-PPGCEM, Federal University of Pelotas, Pelotas, Rio Grande do Sul, Brazil

[4]Shenzhen Institute of Advanced Electronic Materials, Shenzhen Institutes of Advanced Technology, Chinese Academy of Sciences, Shenzhen, China

Correspondence
Cristina Pascual-Gonzalez and Antonio Feteira, Materials and Engineering Research Institute, Sheffield Hallam University, Howard Street, Sheffield S1 1WB, UK.
Email: cristina.pascualg@urjc.es and a.feteira@shu.ac.uk

Funding information
FAPERGS, Grant/Award Number: 19/2551-0001974-2; Carolina Elicker acknowledges CNPq for a SWE Scholarship; Cristina Pascual-González acknowledges Sheffield Hallam University for a VC doctoral scholarship

Abstract

$(1-x)KNbO_3$–$xBiMnO_3$ ($0 \leq x \leq 0.25$) ceramics were prepared by the solid-state reaction method. An X-ray diffraction analysis combined with Raman spectroscopy showed the co-solubility of Bi and Mn in the orthorhombic structure to be less than 5% $BiMnO_3$. Orthorhombic and pseudocubic symmetries coexist in the $0.05 \leq x \leq 0.15$ region, coinciding with a bimodal grain size distribution. This coexistence of crystal symmetries is further corroborated by several anomalies in the dielectric behavior, which can be ascribed to structural phase transitions. For $x \geq 0.20$, only one dielectric anomaly is detected around 100°C, which is commensurate with in situ Raman spectroscopy analysis. This work also shows that Bi/Mn co-doping can be employed to tailor the bandgap of $KNbO_3$, which narrows continuously with increasing x, resulting in ~1-eV narrowing for single-phase $x = 0.25$. This may offer the possibility to employ this ferroic material in photoresponsive technologies.

KEYWORDS
ferroelectricity/ferroelectric materials, Raman spectroscopy, solid solutions

1 | INTRODUCTION

Chemical doping aimed at narrowing the optical bandgaps of classical ferroelectrics such as $KNbO_3$, $BiFeO_3$, and $BaTiO_3$ has recently attracted considerable attention,[1–6] due to the potential use of these materials in the fabrication of photo-responsive devices. Indeed, bandgap narrowing via doping in ferroelectrics has been deemed as an essential footstep for enhancing the photoresponse of ferroelectrics. A few doping strategies were adopted to narrow the bandgap of lead-free ferroelectric $KNbO_3$ as recently reviewed by Wang et al.[7] For example, Grinberg et al.[3]

investigated the $K_{1-x}Ba_xNb_{1-x/2}Ni_{x/2}O_{3-\delta}$, a system where electroneutrality is attained via the creation of oxygen vacancies. These researchers reported a bandgap as low as 1.7 eV for $x = 0.10$; however, it was later demonstrated by Pascual-Gonzalez[8] and by Wu[9] that this low value does not correspond to the intrinsic bandgap, which in reality is only marginally affected by this doping mechanism. This may partially explain the modest photovoltaic performance, such as the short-circuit photocurrent density, J_{sc}, of 0.1 μA/cm^2 and open-circuit photovoltage, V_{oc}, of 0.007 V exhibited at room temperature by a ferroelectric photovoltaic (FEPV) device fabricated from $x = 0.10$. In 2017, it was demonstrated that the optical bandgap of $KNbO_3$ can be successfully reduced by ~1 eV in a virtually defect-free solid solution based in $K_{1-x}Bi_xNb_{1-x}Fe_xO_3$ (KNBF).[10] Later, Elicker et al.[11] observed a comparable bandgap reduction in the $K_{1-x}La_xNb_{1-x}Fe_xO_3$ (KNLF) system, implying a negligible role played by the electronic lone-pair in Bi^{3+} in the process of bandgap narrowing. Their FEPV prototype devices based on KNBF and KNLF ($x = 0.32$) combined with a redox couple (I^-/I^{3-}) displayed a typical diode-like response, characterized by J_{sc} and V_{oc} of 0.115 μA and 0.075 V for KNBF and 0.19 μA and 0.035 V for KNLF, respectively. These are still modest values compared with a more recent study by Li et al.,[12] who fabricated a solar cell based on $(K,Bi)(Nb,Yb)O_3$[13] combined with light-absorbing p-type NiO and TiO_2 nanoparticles. Those cells exhibit a V_{oc} of 1 V, which can be enhanced to 1.56 V via an electric bias close to the coercive field. Under simulated standard AM 1.5G illumination (terrestrial spectra) this cell showed a power conversion efficiency of 0.85%.

To our knowledge, structure–property relationships in the $K_{1-x}Bi_xNb_{1-x}Mn_xO_3$ (KNBM) system remain unexplored. The end-members of this solid solution are the orthorhombic ferroelectric $KNbO_3$ and the monoclinic non-ferroelectric (at least in bulk form) $BiMnO_3$.[14,15] $BiMnO_3$ is known to form solid solutions with other perovskites, which can be prepared at ambient pressure. For example, $Bi_{1-x}La_xMnO_3$[16] can be synthesized at ambient pressure when $x > 0.4$. Woodward and Reaney[17] also showed $BiMnO_3$ to form a solid solution with the ferroelectric $PbTiO_3$, according to the $Pb_{1-x}Bi_xTi_{1-x}Mn_xO_3$ mechanism. Interestingly, the $0.6PbTiO_3$–$0.4BiMnO_3$ composition is characterized by the coexistence of a tetragonal *P*4*mm* phase (isostructural with $PbTiO_3$) and a pseudocubic phase, giving rise to a potentially multiferroic polar/nonpolar morphotropic phase boundary. These examples show $BiMnO_3$ to be an effective putative end-member, which can be employed to tailor physical properties of other stable perovskites. Indeed, it can also provide a promising route to design new photoferroelectrics using a site-by-site substitution approach, which makes use of the stereochemical activity of the $6s^2$ lone-pair of electrons in Bi^{3+}, to create local distortions required to induce polarization, and transition metals to tailor the bandgap. Based on X-ray emission and absorption spectra, McLeod et al.[18] reported a bandgap of 0.9(5) eV for $BiMnO_3$; however, this value should be interpreted with caution, as in the same investigation, the bandgap of $BiFeO_3$ was reported as 0.9 eV, when literature's widely accepted value is ~2.7 eV.[19–21] Bhardwaj et al.[22] prepared $BiMnO_3$ by sol–gel and reported a bandgap of 1.25 eV. Xu et al.[23] reported a bandgap of 1.1 eV for epitaxial thin films fabricated from $BiMnO_3$. Interestingly, they also demonstrated that $BiMnO_3$ can be employed to narrow down the bandgap of $BiFeO_3$, in agreement with a previous study by Bi et al.[24] Hence, based on an empirical mixing approach, one may expect $BiMnO_3$ to be an effective end-member to reduce the bandgap of $KNbO_3$, providing that a solid solution between the two compounds is thermodynamically viable.

In this work, the effect of $BiMnO_3$ alloying on the long-range polar order of $KNbO_3$ is investigated for the first-time using Raman spectroscopy, whereas the impact of this alloying mechanism on the optical bandgap is investigated by UV–visible (UV–VIS) diffuse reflectance spectroscopy. To our knowledge, the structure–property relationships in the $KNbO_3$–$BiMnO_3$ system have never been investigated.

2 | EXPERIMENTAL PROCEDURES

KNBM ($0 \leq x \leq 0.25$) ceramics were fabricated by the solid-state reaction method. Oxides and carbonates were pre-dried in a drying oven at 200°C for 24 h to avoid any unwanted moisture. High-purity K_2CO_3 (Sigma-Aldrich, >99%), Nb_2O_5 (Aldrich, 99.9%), Bi_2O_3 (Fluka Analytical, 98%), and Mn_2O_3 (Aldrich, 99%) powders were weighed in the required stoichiometric ratios to produce 15 g of each composition. The mixture was placed into a polyethylene bottle containing propanol (up to 50 ml) and Y-stabilized zirconia milling media. Then, the bottle was transferred into a ball mill and rotated overnight (for 24 h) for effective mixing of the reactants. After milling, the slurry was moved into a stainless-steel pan, which was placed into the drying oven at 100°C. The mixed powders were passed through a 250-μm mesh sieve. Sieved powders were placed into covered alumina crucible and fired at 800°C in air for reaction for 4 h using a heating rate of 3°C/min. The powders were re-milled, and the calcination repeated at 900°C, in order to ensure that reaction proceeds to completion. The end of the processing was considered when non-changes in the X-ray diffraction (XRD) were observed. Subsequently, pellets of 10 mm in diameter and ~2 mm in thickness were fabricated by uniaxial pressing (1 ton). Higher applied pressure loads led to the appearance of cracks in the pellets. Green bodies were sintered in air for

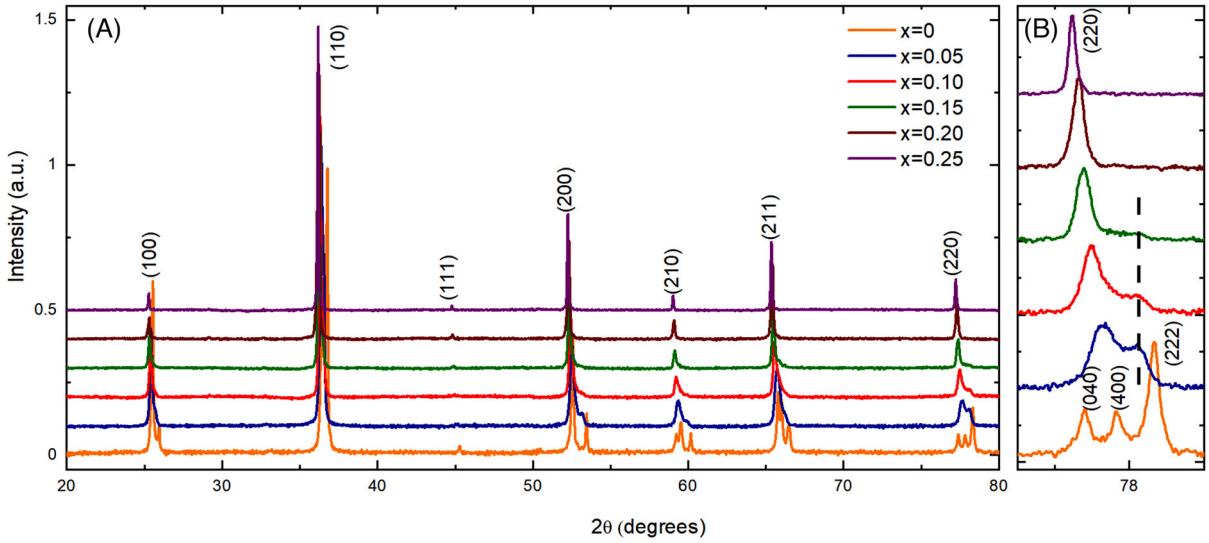

FIGURE 1 The room-temperature X-ray diffraction (XRD) data for KNBM ($0 \leq x \leq 0.25$) ceramics sintered at 1070°C for 4 h in the (A) $20 \leq 2\theta \leq 80$ range and (B) around 78° 2θ

4 h at 1070°C using a controlled heating rate of 3°C/min. No binder was used.

Phase purity and crystal structure were evaluated by powder XRD using a PANalytical diffractometer equipped with a Co-tube ($\lambda = 1.7890$ Å, model Empyrean). Data were collected in the 2θ range 20°–80°, with a step size of 0.02° with a scan length of 2 s/step. Raman spectra were obtained with a Renishaw Raman microscope (model InVia) using a 532-nm solid state (100 mW) laser, in backscattering geometry. In situ temperature Raman spectroscopy was carried out using a Linkam stage (model THMS600). A scanning electron microscope (model: Nova Nano 200, FEI, Brno, Czech Republic) equipped with a field emission gun was used to examine the ceramic microstructures. EDX mapping of K, Nb, Bi, and Mn was carried out. In order to measure the electrical properties, electrodes were fabricated from Pt painted onto both faces of the ceramic discs and heat-treated at 600°C for 30 min. Relative permittivity was extracted from temperature-dependent capacitance measurements in the frequency range 10 kHz–1 MHz using an Agilent LCR meter (model E4980A) and employing a small signal of 100 mV. A heating rate of 1°C/min was employed. Finally, DRUV–vis spectra were acquired in the range 200–1400 nm using a Shimadzu UV–VIS–NIR spectrophotometer (model UV-3600 Plus). Fine $BaSO_4$ powder was employed as a non-absorbing standard. To estimate the bandgaps, the Kubelka–Munk (K–M) function given in the following was first calculated:

$$F\ (R) = \frac{(1-R)^2}{2R}$$

where R is the experimental reflectance referred to a $BaSO_4$ standard. Hereafter, the K–M function (or $F(R)$ curves) is assumed to be proportional to the optical absorption. Therefore, the absorption coefficient, α, can be replaced by $F(R)$ in the Tauc equation:

$$(h\nu\alpha)^n = A\ (h\nu - E_g) = [h\nu F\,(R)]^n$$

where h is Planck's constant, ν is frequency of vibration, α is absorption coefficient, E_g is the bandgap, and A is a proportionality constant. For direct allowed transition, $n = 2$ and for indirect allowed transition, $n = 1/2$.

3 | RESULTS AND DISCUSSION

3.1 | Phase purity and crystal structure

The room-temperature XRD data for KNBM ($0 \leq x \leq 0.25$) ceramics sintered at 1070°C for 4 h are shown in Figure 1. XRD data for undoped KN can be assigned to an orthorhombic perovskite described by the $Amm2$ space group. The lattice parameters of KN were refined as $a = 3.9711(1)$ Å, $b = 5.6909(1)$ Å, and $c = 5.7158(1)$ Å, which are in good agreement with those reported on ICDD card 00-032-0822. For $x \geq 0.05$, the absence of reflections associated with any secondary phase or residual precursor phases supports the incorporation of Bi^{+3} and Mn^{+3} into two KN-based phases, as described later. The peak splitting typical for the orthorhombic structure disappears gradually with increasing alloying levels and new reflections ascribed to a new KN-based pseudocubic phase appear. For doped KNBM ceramics (up $x = 0.10$), the orthorhombic a lattice parameter increases, whereas c decreases, as shown by the data listed in Table 1. For

TABLE 1 Rietveld refinement results for KNBM $x = 0$, $x = 0.05$, $x = 0.10$, $x = 0.15$, $x = 0.20$, and $x = 0.25$ ceramics

x	0	0.05		0.10		0.15		0.20	0.25
Space group	*Amm*2	*Amm*2 22.8(7) %	*Pm*$\bar{3}$*m* 77.2(1) %	*Amm*2 14.1(5) %	*Pm*$\bar{3}$*m* 85.9(1) %	*Amm*2 5.4(3) %	*Pm*$\bar{3}$*m* 94.6(8) %	*Pm*$\bar{3}$*m*	*Pm*$\bar{3}$*m*
Density (experimental) g/cm^3	4.35(3)	4.3(2)		4.2(1)		4.3(2)		4.3(2)	4.2(1)
Density (calculated) g/cm^3	4.6273(1)	4.7829(7)	4.7568(4)	4.9560(8)	4.8890(2)	5.1267(7)	5.0480(2)	5.2137(4)	5.3657(9)
Relative density (%)	94(1)	91(4)[a]		86(2)[a]		85(5)[a]		83(3)[a]	78(1)[a]
***a* (Å)**	3.9711(1)	3.9883(3)	4.0234(2)	4.0003(3)	4.0325(1)	3.9874(3)	4.0353(1)	4.0356(8)	4.0406(1)
***b* (Å)**	5.6909(1)	5.6979 (6)	4.0234(2)	5.6855(5)	4.0325(1)	5.6800(7)	4.0353(1)	4.0356(8)	4.0406(1)
***c* (Å)**	5.7158(1)	5.7007(5)	4.0234(2)	5.6914(6)	4.0325(1)	5.7176(8)	4.0353(1)	4.0356(8)	4.0406(1)
V/10^6 (pm^3)	64.576(2)	64.77(1)	65.130(7)	64.72(1)	65.572(3)	64.748(10)	65.711(3)	65.723(3)	65.97(1)
R_{exp}	1.26460	0.69640		0.84829		0.83353		0.6694	0.68507
$R_{profile}$	2.97912	1.34817		2.17999		2.27072		1.54564	1.33107
R_{wp}	4.65175	1.91855		3.16955		3.85881		2.48361	2.22667
GOF	13.53086	7.58975		13.96061		21.43187		13.76548	10.56425

[a]Relative densities were calculated with the ratio of the theoretical densities from the two coexisting phases.

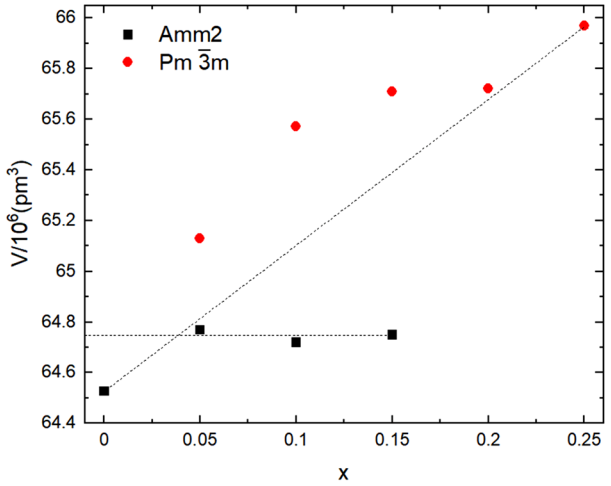

FIGURE 2 Compositional variation of the unit cell volume for KNBM $0 \leq x \leq 0.25$ ceramics

the pseudocubic phase, the lattice constant increases from 4.0234(2) Å for $x = 0.05$ to 4.0406(1) Å for $x = 0.25$.

These reflections shift toward lower 2θ angles, indicating an increase of the unit cell volume with increasing Bi^{3+}/Mn^{3+} contents. The variations of the unit cell volumes with increasing x for the orthorhombic and cubic phases are illustrated in Figure 2. This variation is consistent with the replacement of Nb^{5+} ($r_{VI} = 0.64$ Å) by the larger Mn^{3+} ($r_{VI} = 0.645$ Å), which under the assumption of a high spin state, may give rise to a Jahn–Teller distortion. The presence of larger Mn^{2+} should not be discarded, as this cation in sixfold coordination has an even larger radius ($r_{VI} = 0.67$ and 0.83 Å, for low- and high-spin, respectively).

A closer inspection of the XRD data suggests the coexistence of two KN-based polymorphs. Indeed, with increasing x, the triplet between 77° and 80° ($x = 0$) evolves into a single peak accompanied by a significant reduction of intensity for the reflection at higher 2θ angles (Figure 1B), which eventually disappears at $x = 0.20$. Speculatively, this reflection (black dashed line, Figure 1B) can be ascribed to an orthorhombic KN-based phase (reflection (2 2 2) for $x = 0$).

Moreover, in comparison with undoped KN, this reflection is slightly shifted toward lower 2θ angles, as a result of simultaneous incorporation of Bi^{+3} and Mn^{+3}. The fact that this reflection does not shift for $x > 0.05$ suggests that the solubility limit in orthorhombic KN structure is limited to $x \leq 0.05$. This is supported by the Rietveld refinements in Table 1, which show XRD data for $0.05 \leq x \leq 0.15$ to be successfully refined as a combination of an orthorhombic phase (space group *Amm*2) and cubic phase (space group *Pm*$\bar{3}$*m*). The calculated content of cubic phase increases from ~77% for $x = 0.05$ to ~95% for $x = 0.15$. Finally, reflections associated with the orthorhombic polymorph are not visible in KNBM $x = 0.20$ and $x = 0.25$, which is consistent with an average cubic structure. The orthorhombic phase for $0.05 \leq x \leq 0.15$ presents an average unit cell volume of ~64.7 Å^3 (indicated by a horizontal dashed black line in Figure 2). This fact suggests limited incorporation of Bi^{3+}/Mn^{3+} into the orthorhombic phase. On the other hand, the volume of the cubic phase increases with x;

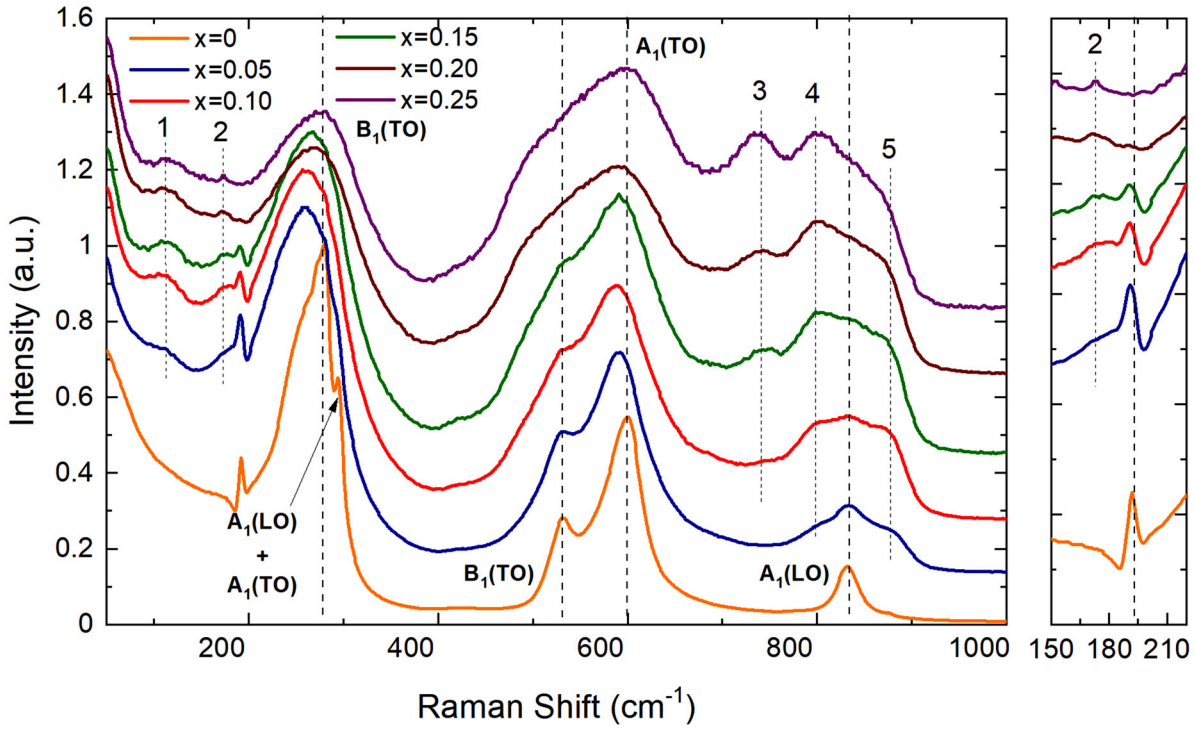

FIGURE 3 Room-temperature Raman spectra for KNBM $0 \leq x \leq 0.25$ ceramics

however, in the $0.05 \leq x \leq 0.15$ range, this variation is nonlinear, which may be associated with inhomogeneous dopant incorporation, as inferred from the EDX maps of K, Nb, Bi, and Mn for $x = 0.05$ and $x = 0.25$ ceramics shown in Figures S3 and S4. Additional XRD data for KNBM $x = 0$, 0.01, 0.02, 0.04 and $x = 0.08$ can be found in Figure S1. The reduction in orthorhombicity and the emergence of the cubic phase becomes evident.

3.2 | Raman spectroscopy

Room-temperature Raman spectra for KNBM $0 \leq x \leq 0.25$ ceramics are illustrated in Figure 3. The assignment of Raman modes for pure KN follows the classical work by Quittet et al.[25] Essentially, all doped compositions exhibit the same general spectral features observed in undoped KN; however, those modes are broader (which can be directly related to a higher degree of disorder) and slightly shifted toward lower wave numbers. In addition, new modes emerge in all doped compositions, which are labeled as 1,2,3,4, and 5. Mode 1 appears around ~100 cm^{-1} and mode 2 emerges at ~175 cm^{-1} as a shoulder of the sharp peak at 192 cm^{-1}. Their intensity increases systematically with increasing the co-substitution of Bi and Mn, but they do not exhibit any frequency shift. Comparable modes have been reported in the $KNbO_3$–$BiFeO_3$ system,[10] which were speculatively associated to A–O vibrations within nm-sized clusters rich in either Bi^{3+} and/or K^+ cations. The sharp mode at 192 cm^{-1} is invariably regarded as a fingerprint for the occurrence of long-range polar order in KN; its perceptibility in the spectra of compositions up to $x = 0.15$ is in broad agreement with the XRD data that suggest the presence of a residual orthorhombic KN-based phase (ferroelectric phase) in $x = 0.15$. Indeed, the intensity of this sharp mode decreases with increasing x, in agreement with a decline of the content of the orthorhombic phase in KNBM ($0.05 \leq x \leq 0.15$) ceramics, as estimated from the Rietveld refinements, in Table 1.

Modes 3 and 4 appear at 740 and 800 cm^{-1}, respectively, and their relative intensity increases with increasing x. Finally, mode 5, the least intense, continuously shifts by ~10 cm^{-1} to lower wave numbers. The absence of the sharp mode at 192 cm^{-1} for $x \geq 0.20$, is consistent with the disappearance of ferroelectric orthorhombic KN-based phases, but the presence of Raman modes for $x \geq 0.20$ shows that the local structure is not purely cubic, as Raman activity is absent from crystals described by the centrosymmetric $Pm\bar{3}m$ space group. Raman spectroscopy data for $x \leq 0.08$ are given in Figure S2 of the ESI. For $x \leq 0.04$, all spectra exhibit spectral features like those of orthorhombic KN, with the addition of a small intensity mode adjacent to the A_1(LO) mode. The A_1(LO) + A_1(TO) mode softens continuously with increasing x.

In summary, the evolution of the room-temperature Raman spectra is consistent with the XRD analysis. In

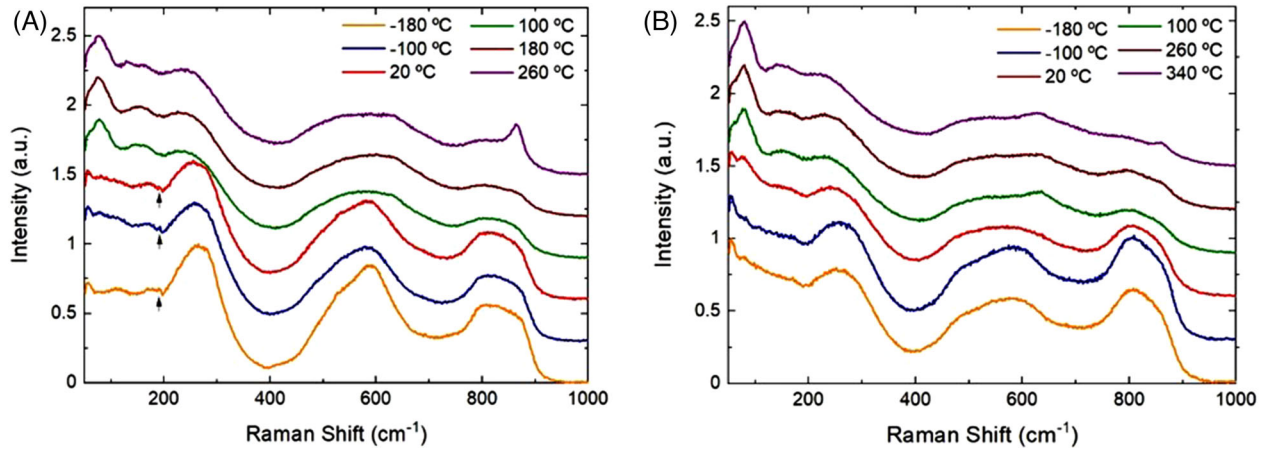

FIGURE 4 In situ Raman spectroscopy for KNBM ceramics: (A) $x = 0.15$ and (B) $x = 0.25$

addition, in situ temperature-dependent Raman spectroscopy was conducted to gather a further insight into the nature of the coexisting phases. For this purpose, a biphasic composition ($x = 0.15$) and a single-phase composition ($x = 0.25$) were investigated. The results are illustrated in Figure 4, which clearly show a dramatic change in the Raman spectra between 20 and 100°C, marked by the appearance of a sharp mode below 100 cm^{-1}.

A more detailed analysis confirms the presence of a spectral feature (as indicated by the arrows) associated with a polar phase for $x = 0.15$ in the temperature range between −180 and 20°C, as shown in Figure 4A. This feature is absent from all the spectra for $x = 0.25$, as shown if Figure 4B. New modes also appear at 620 and 900 cm^{-1} in both compositions above 100°C. The modification of the Raman activity supports the fact that the room-temperature structure is pseudocubic, and this is also consistent with a dielectric anomaly around 100°C, as it will be shown later in Section 3.4.

At this stage, it is useful to reiterate that in the KNBM system, the co-solubility of Bi and Mn in the orthorhombic phase is limited to $x < 0.05$. In the $0.05 \leq x \leq 0.15$ compositional range, the orthorhombic phase coexists with a pseudocubic phase, as shown by XRD and Raman spectroscopy. Finally, both $x = 0.20$ and 0.25 exhibit a pseudocubic structure that undergoes a transformation between 20 and 100°C, as shown by Raman spectroscopy.

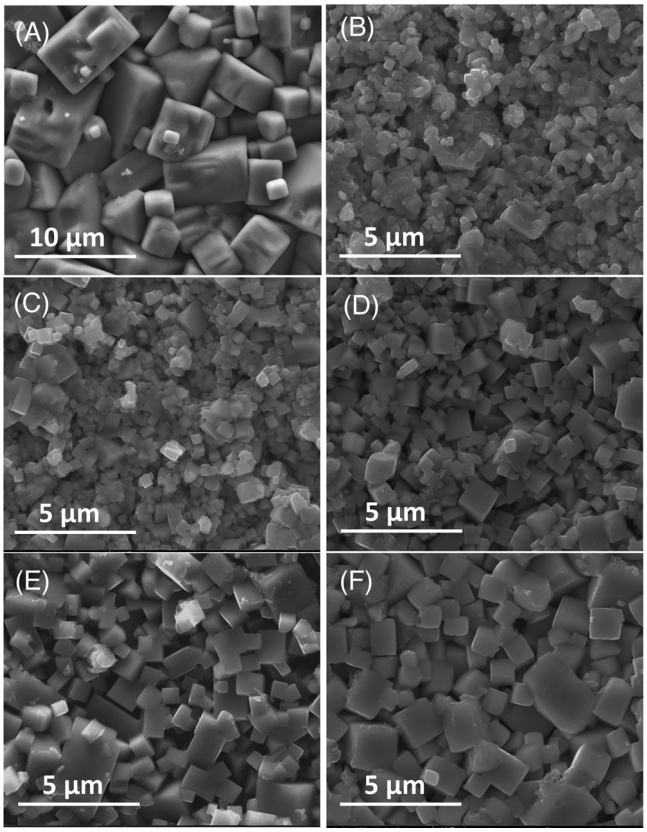

FIGURE 5 Microstructures for KNBM ceramics: (A) $x = 0$, (B) $x = 0.05$, (C) $x = 0.10$, (D) $x = 0.15$, (E) $x = 0.20$, and (F) $x = 0.25$

3.3 | Phase assemblage and microstructure

Scanning electron microscopy images of the as-fired surfaces for KBMN ceramics are illustrated in Figure 5. The microstructure of undoped KN consists of cubic grains, with sizes varying between 3 and 5 μm. Bimodal microstructures consisting of a mixture of cubic grains embedded in a matrix of fine irregularly shaped grains were observed for KBMN ceramics in the $0.05 \leq x \leq 0.15$ range, as shown in Figure 5B–D. Coincidentally this type of microstructure is only observed within the compositional range where two phases coexist, as revealed by XRD in Figure 2. After an initial grain size reduction upon doping,

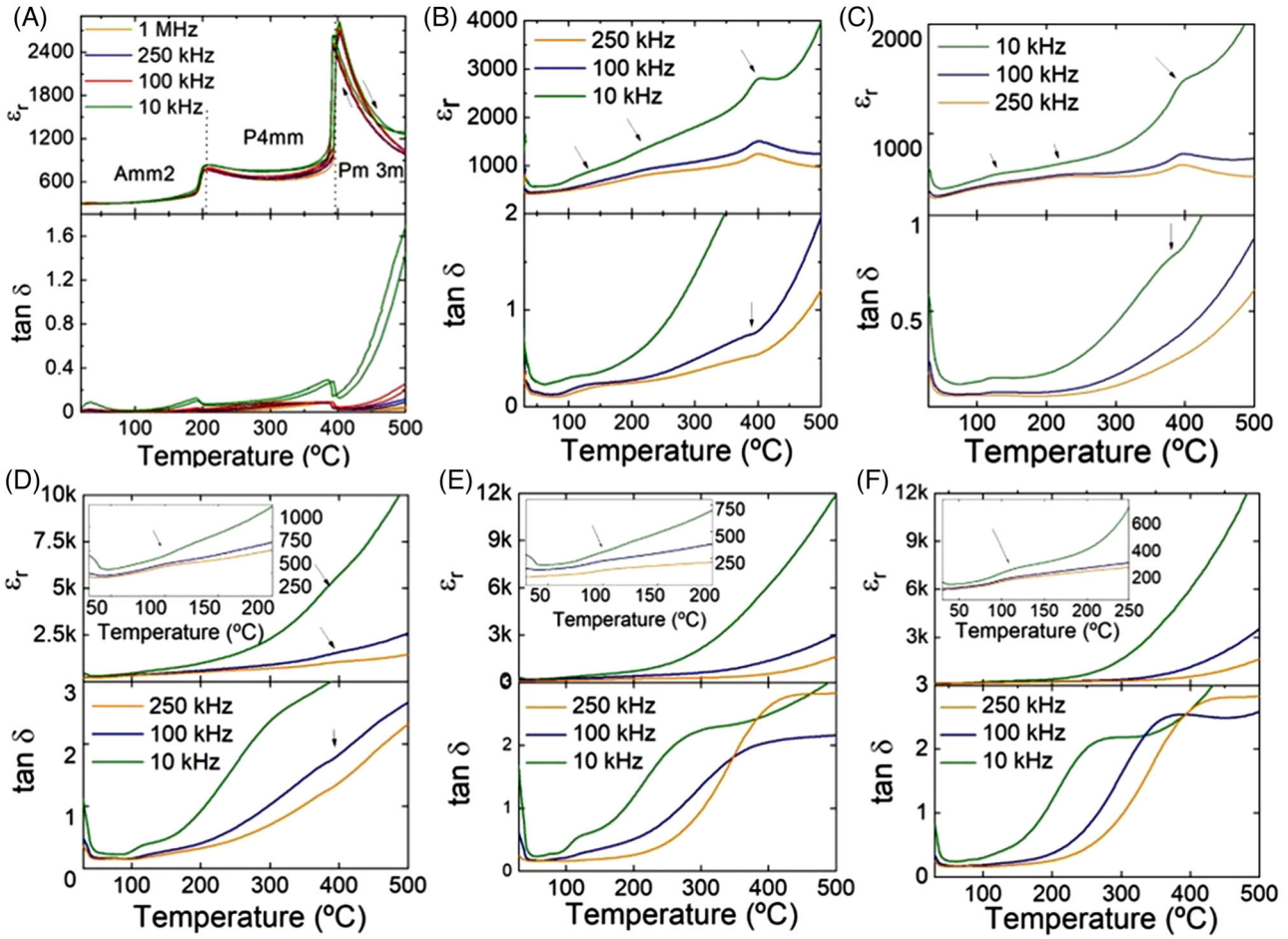

FIGURE 6 Temperature dependences of relative permittivity and loss tangent for KNBM ceramics: (A) $x = 0$, (B) $x = 0.05$, (C) $x = 0.10$, (D) $x = 0.15$, (E) $x = 0.20$, and (F) $x = 0.25$

the grain size increases continuously and ceramics with $x \geq 0.2$ consist uniquely of cubic grains with an average grain size greater than 1 μm.

3.4 | Dielectric properties

Temperature dependence of the relative permittivity (ε_r) and loss tangent (tan δ) for KNBM ceramics ($x = 0$, 0.05, 0.10, 0.15, 0.20, and 0.25) measured at 10, 100, and 250 kHz are illustrated in Figure 6. Undoped KN shows two large dielectric anomalies at 206 and 394°C, corresponding to the orthorhombic–tetragonal and tetragonal-to-cubic transitions, respectively, as illustrated in Figure 6A. These dielectric anomalies are also visible in $x = 0.05$ and $x = 0.10$ at ~220 and ~400°C, as illustrated in Figure 6B,C, respectively. Their presence corroborates the presence of the orthorhombic ferroelectric phase as determined from the XRD and Raman analysis (Figures 1 and 3, respectively). A third anomaly around 100°C (indicated with an arrow) is also visible. Again, its presence is consistent with the in situ Raman spectroscopy analysis in Figure 4, which reveals a local structural modification in this temperature range. The temperature for the ε_r anomalies remains almost constant, but their magnitude decreases with frequency. KNBM $x = 0.15$ shows a dielectric anomaly at ~400°C, which is indicated with an arrow, as shown in Figure 6D. Again, this is consistent with the 5% of orthorhombic phase estimated by Rietveld refinement for KNBM $x = 0.15$.

For compositions with $x \geq 0.20$, only one dielectric anomaly is observed around 100°C, as illustrated in Figure 6E,F for $x = 0.20$ and $x = 0.25$, respectively. Again, this is in broad agreement with the in situ Raman data shown in Figure 4B for $x = 0.25$. Finally, it is worth to mention that the dramatic increase of the loss tangent with increasing temperature is associated to an increase of the electrical conductivity.

3.5 | Diffuse reflectance spectroscopy

Diffuse reflectance spectroscopy was carried out in the range of 200–1400 nm. Bandgaps can be obtained from the intersection of the tangent line in the plot of $[h(R)]^n$

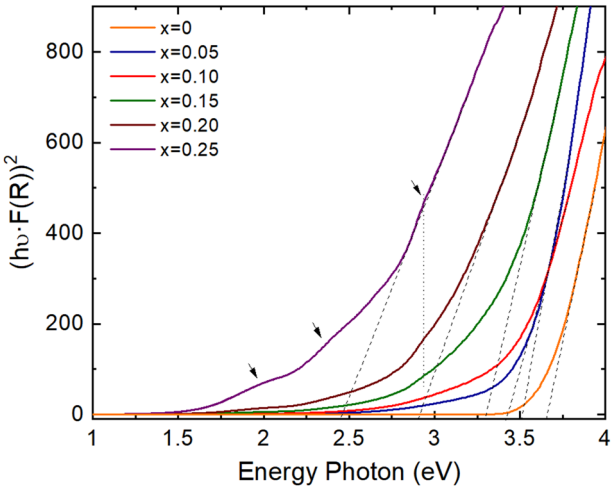

FIGURE 7 Tauc plot spectra for KNBM $0 \leq x \leq 0.25$ ceramics

with the x-axis; $F(R)$ is the K–M function, and R are the diffuse reflectance data. Figure 7 shows the Tauc plot of KNBM $0 \leq x \leq 0.25$ ceramics constructed for $n = 2$ (direct bandgap). Bandgaps narrow systematically from 3.66 eV ($x = 0$) to 2.44 eV ($x = 0.25$).

The estimation of the bandgaps was done by the Tauc method, which for the case of the single-phase materials should not pose an issue. Hence, for $x = 0$, $x = 0.20$ and 0.25, the estimated values should be rather accurate. The accuracy of the bandgaps for the non-single phase materials is affected by the coexistence of two different phases, but we did not see a clear superposition of spectra that could be ascribed to each phase, which could be employed to use a subtraction method to extract the bandgap for each phase. The arrows indicate the absorption at lower energies, which can be ascribed to intrabandgap states or inhomogeneities, and it would be incorrect to fit tangents to those regions to estimate the intrinsic optical bandgap. The nonlinear dependence of the bandgap with x may also be a result of chemical non-homogeneity, associated mainly with the different solubility limits of the coexisting orthorhombic and pseudocubic phases, but also to some residual Mn-rich phase, which remained undetected in the XRD analysis, but can be observed in the EDX mapping provided in Figures S3 and S4. Finally, we reiterate that $x = 0.20$ and 0.25 are only pseudocubic, as demonstrated by the Raman spectra, thereby at local level these are non-cubic semiconductors.

4 | CONCLUSIONS

In this work, the structure–composition–properties relationships of $(1 - x)KNbO_3$–$xBiMnO_3$ ($0 \leq x \leq 0.25$) ceramics were established by combining XRD, Raman spectroscopy, and electron microscopy with dielectric and optical measurements. It was found that the co-solubility of Bi and Mn into the orthorhombic phase of KN is limited to $x < 0.05$. This is accompanied by a small increase in the temperature of the orthorhombic–tetragonal structural phase transition from 206 to 220°C, and of the tetragonal–cubic phase transition from 394 to 400°C. In the $0.05 \leq x \leq 0.15$ region, ceramics consist of a combination of orthorhombic and pseudocubic phases. In this compositional range, the volume of the unit cell of the pseudocubic phase increases from 65.130(7) to 65.711(3) Å^3, corroborating the incorporation of Bi and Mn in this pseudocubic lattice. This also implies a nonhomogeneous distribution of dopants between those phases, which has an impact on the optical response of these materials, making it more challenging to extract a single-bandgap value. For $x \geq 0.20$, XRD data can be refined as a cubic single-phase, but Raman spectroscopy shows that their local structure is non-cubic. The room-temperature relative permittivity of these high dopant content ceramics is around 200, which is greater than that one would expect for a cubic perovskite, therefore supporting the pseudocubic nature of the compositions $x = 0.20$ and 0.25. Interestingly, in situ Raman spectroscopy suggests the occurrence of a possible structural transition around 100°C, which is in broad agreement with a subtle dielectric anomaly observed in the temperature dependence of the relative permittivity. Finally, the direct bandgap for undoped $KNbO_3$ is 3.66 eV, whereas for $x = 0.25$, it narrows to 2.44 eV, as confidently estimated from diffuse reflectivity data, as those are single-phase compositions. This narrowing of the bandgap by more than 1 eV opens the potential to exploit these ferroic materials in photoresponsive process.

ACKNOWLEDGMENTS

The authors are thankful to CNPq, CAPES, and FAPERGS (Grant no. 19/2551-0001974-2) for financial support. Carolina Elicker acknowledges CNPq for a SWE Scholarship (Process no. 201665/2015-8). Cristina Pascual-González acknowledges Sheffield Hallam University for a VC doctoral scholarship. Antonio Feteira is thankful to CNPq for a Special Visiting Researcher Fellowship. Dr Giorgio Schileo is acknowledged for the reflectance measurements.

ORCID

Mario L. Moreira https://orcid.org/0000-0002-0588-3717
Sergio Cava https://orcid.org/0000-0002-0907-7739
Dawei Wang https://orcid.org/0000-0001-6957-2494
Antonio Feteira https://orcid.org/0000-0001-8151-7009

REFERENCES

1. Kreisel J, Alexe M, Thomas PA. A photoferroelectric material is more than the sum of its parts. Nat Mater. 2012;11(4):260.
2. Yang MM, Luo ZD, Kim DJ, Alexe M. Bulk photovoltaic effect in monodomain $BiFeO_3$ thin films. Appl Phys Lett. 2017;110(18):5.

3. Grinberg I, West D, Torres M, Gou G, Stein D, Wu L, et al. Perovskite oxides for visible-light-absorbing ferroelectric and photovoltaic materials. Nature. 2013;503(7477)509–12.
4. Si SF, Deng HM, Zhou WL, Wang TT, Yang PX, Chu JH. Modified structure and optical band-gap in perovskite ferroelectric (1-x)$KNbO_3$-x$BaCo_{1/3}Nb_{2/3}O_3$ ceramics. Ceram Int. 2018;44(12):14638–44.
5. Yu L, Jia J, Yi G, Shan Y, Han M. Bandgap tuning of [$KNbO_3$](1-x)[$BaCo_{1/2}Nb_{1/2}O_{3-\delta}$](x) ferroelectrics. Mater Lett. 2016;184:166–8.
6. Nechache R, Harnagea C, Li S, Cardenas L, Huang W, Chakrabartty J, et al. Bandgap tuning of multiferroic oxide solar cells. Nat Photon. 2015;9(1):61–7.
7. Wang DW, Wang G, Lu ZL, Al-Jlaihawi Z, Feteira A. Crystal structure, phase transitions and photoferroelectric properties of $KNbO_3$-based lead-free ferroelectric ceramics: a brief review. Front Mater. 2020;7:91.
8. Pascual-Gonzalez C. Processing-composition-structure effects on the optical band gap of $KNbO_3$-based ceramics. PhD Thesis. Sheffield Hallam University; 2017.
9. Wu L. Investigation of ferroelectric perovskite oxides for photovoltaic applications. PhD Thesis. University of Pennsylvania; 2019.
10. Pascual-Gonzalez C, Schileo G, Murakami S, Khesro A, Wang DW, Reaney IM, et al. Continuously controllable optical band gap in orthorhombic ferroelectric $KNbO_3$-$BiFeO_3$ ceramics. Appl Phys Lett. 2017;110(17):172902.
11. Elicker C, Pascual-Gonzalez C, Gularte LT, Moreira ML, Cava SS, Feteira A. Photoresponse of $KNbO_3$-$AFeO_3$ (A = Bi^{3+} or La^{3+}) ceramics and its relationship with bandgap narrowing. Mater Lett. 2018;221;326–9.
12. Li C, Jiang K, Jiang J, Hu Z, Liu A, Hu G, et al. Enhanced photovoltaic response of lead-free ferroelectric solar cells based on (K,Bi)(Nb,Yb)O_3 films. Phys Chem Chem Phys. 2020;22(6):3691–701.
13. Pascual-Gonzalez C, Schileo G, Feteira A. Band gap narrowing in ferroelectric $KNbO_3$-Bi(Yb,Me)O_3 (Me = Fe or Mn) ceramics. Appl Phys Lett. 2016;109(13):132902.
14. Goian V, Kamba S, Savinov M, Nuzhnyy D, Borodavka F, Vaněk P, et al. Absence of ferroelectricity in $BiMnO_3$ ceramics. J Appl Phys. 2012;112(7):074112.
15. Belik AA. Polar and nonpolar phases of $BiMO_3$: a review. J Solid State Chem. 2012;195:32–40.
16. Troyanchuk IO, Mantytskaja OS, Szymczak H, Shvedun MY. Magnetic phase transitions in the system $La_{1-x}Bi_xMnO_{3+\delta}$. Low Temp Phys. 2002;28(7):569–73.
17. Woodward DI, Reaney IM. A structural study of ceramics in the $BiMnO_3$(x)-$PbTiO_3$(1-x) solid solution series. J Phys Condens Matter. 2004;16(49):8823–34.
18. McLeod JA, Pchelkina ZV, Finkelstein LD, Kurmaev EZ, Wilks RG, Moewes A, et al. Electronic structure of $BiMO_3$ multiferroics and related oxides. Phys Rev B. 2010;81(14):144103.
19. Basu SR, Martin LW, Chu YH, Gajek M, Ramesh R, Rai RC, et al. Photoconductivity in $BiFeO_3$ thin films. Appl Phys Lett. 2008;92(9):091905.
20. Ihlefeld JF, Podraza NJ, Liu ZK, Rai RC, Xu X, Heeg T, et al. Optical band gap of $BiFeO_3$ grown by molecular-beam epitaxy. Appl Phys Lett. 2008;92(14):142908.
21. Xu XS, Brinzari TV, Lee S, Chu YH, Martin LW, Kumar A, et al. Optical properties and magnetochromism in multiferroic $BiFeO_3$. Phys Rev B. 2009;79(13):134425.
22. Bhardwaj N, Gaur A, Yadav K. Effect of doping on optical properties in $BiMn_{1-x}(TE)_xO_3$ (where x = 0.0, 0.1 and TE = Cr, Fe, Co, Zn) nanoparticles synthesized by microwave and sol-gel methods. Appl Phys A: Mater Sci Process. 2017;123(6):7.
23. Xu XS, Ihlefeld JF, Lee JH, Ezekoye OK, Vlahos E, Ramesh R, et al. Tunable band gap in $Bi(Fe_{1-x}Mn_x)O_3$ films. Appl Phys Lett. 2010;96(19):192901.
24. Bi L, Taussig AR, Kim HS, Wang L, Dionne GF, Bono D, et al. Structural, magnetic, and optical properties of $BiFeO_3$ and Bi_2FeMnO_6 epitaxial thin films: an experimental and first-principles study. Phys Rev B. 2008;78(10):104106.
25. Quittet A, Bell M, Krauzman M, Raccah P. Anomalous scattering and asymmetrical line-shapes in Raman-spectra of orthorhombic $KNbO_3$. Phys Rev B. 1976;14(11):5068–72.

SUPPORTING INFORMATION

Additional supporting information can be found online in the Supporting Information section at the end of this article.

How to cite this article: Pascual-Gonzalez C, Elicker C, Moreira ML, Cava S, Sterianou I, Wang D, et al. Crystal structure, dielectric properties, and optical bandgap control in $KNbO_3$–$BiMnO_3$ ceramics. J Am Ceram Soc. 2022;1–9. https://doi.org/10.1111/jace.18779